Next Materials 8 (2025) 100777

Contents lists available at ScienceDirect

Next Materials

journal homepage: www.sciencedirect.com/journal/next-materials

Research article

Synthesis of mesoporous SiO_2–Al_2O_3 hollow spheres using ultrasonic irradiation and their activity for hydrolysis of ammonia borane

Naoki Toyama [a,*], Takehiro Nagashima [a], Kaori Wada [b], Kenzo Deguchi [c], Shinobu Ohki [c], Yuuki Mogami [c], Masataka Tansho [c], Atsushi Goto [c], Shigeki Furukawa [a]

[a] Department of Sustainable Engineering, College of Industrial Technology, Nihon University, 1-2-1, Izuni-cho, Narashino, Chiba 275-8575, Japan
[b] Department of Applied Chemistry, Institute of Science and Engineering, Chuo University, 1-13-27 Kasuga, Bunkyo-ku, Tokyo 112-8551, Japan
[c] National Institute for Materials Science, 3-13, Sakura, Tsukuba, Ibaraki 305-0003, Japan

ARTICLE INFO

Keywords:
Mesoporous
Hollow spheres
Silica–alumina
Ammonia borane
Ultrasonic irradiation

ABSTRACT

In this study, mesoporous silica–alumina (SiO_2–Al_2O_3) hollow spheres (HSs) were synthesized through ultrasonic irradiation and evaluated in terms of their activity for the hydrolysis of ammonia borane (NH_3BH_3). The mesoporous SiO_2–Al_2O_3 HSs were formed using a sol–gel method under ultrasonic irradiation using polystyrene particles as templates. We synthesized the samples at ultrasonic irradiation times for 0, 3, and 6 h. The morphologies of the samples were observed using transmission electron microscopy. The shell thickness of the samples increased with increasing ultrasonic irradiation time. In ^{27}Al solid-state nuclear magnetic resonance spectra, the sample with ultrasonic irradiation for 6 h showed the highest proportion of 4-coordinated aluminum species attributed to aluminum in the silica network and the lowest proportion of 5-coordinated aluminum species attributed to amorphous aluminum. The activity for hydrolysis of NH_3BH_3 was determined at room temperature in the presence of the samples with ultrasonic irradiation for 0, 3, and 6 h. According to the results, 7.7-, 10.6-, and 12.3-mL hydrogen were finally generated in the presence of the samples with ultrasonic irradiation for 0, 3, and 6 h, respectively. These results indicate that the amount of hydrogen evolution increased with increasing ultrasonic irradiation time. Furthermore, the amount of hydrogen evolution depended on the number of acid sites of the samples measured using the neutralization titration method. Meanwhile, the reaction time to complete hydrogen generation increased as the ultrasonic irradiation time of the samples increased. Therefore, we measured the pore size distribution of the samples using N_2 adsorption–desorption measurement. The samples with ultrasonic irradiation for 0, 3, and 6 h had peaks at approximately 2.4, 2.1, and a value smaller than 1.4 nm nm, respectively. From these results, the mesopore size of the samples decreased with increasing ultrasonic irradiation time. This result might be related to the number of mesopores formed on the shell of the HSs.

1. Introduction

Amorphous silica–alumina (SiO_2–Al_2O_3) is widely utilized solid acid catalyst for various chemical reactions, such as hydrocracking, isomerization, and alkylation in the petrochemical industry [1–6]. Amorphous SiO_2–Al_2O_3 forms acid sites when aluminum (Al) substitutes for silicon (Si) in the SiO_2 structure. The selectivity and reactivity of catalytic activities depend on the strength and number of acid sites of amorphous SiO_2–Al_2O_3 [6]. On this basis, the development of technologies that can design and synthesize various structures of acid sites is promising. For instance, amorphous SiO_2–Al_2O_3 has a random structure, producing various acid sites [6].

Our group previously applied amorphous SiO_2–Al_2O_3 for the hydrolysis of ammonia borane (NH_3BH_3) [7,8]. NH_3BH_3 has attracted attention as a chemical hydrogen storage material because of its high hydrogen storage density (19.6 mass%), nontoxicity, and chemical stability [9–11]. Hydrogen gas was obtained through a hydrolysis reaction from NH_3BH_3 at room temperature using catalysts [12–16]. Recently, it has been reported that catalysts with hollow and yolk-shell structures show high activity for this reaction [17–20]. We found that amorphous SiO_2–Al_2O_3 hollow spheres (HSs) show much higher activity than SiO_2–Al_2O_3 fine particles and spherical SiO_2–Al_2O_3 particles [21].

* Corresponding author.
E-mail address: toyama.naoki@nihon-u.ac.jp (N. Toyama).

https://doi.org/10.1016/j.nxmate.2025.100777
Received 1 February 2025; Received in revised form 9 April 2025; Accepted 27 May 2025
Available online 4 June 2025

Additionally, we revealed that the hydrolysis of NH_3BH_3 depends on the acid sites of samples [22,23]. From the viewpoint of synthetic material, it is important to determine the acid sites structure of the SiO_2–Al_2O_3 HSs, but this problem remains a difficult challenge because of the amorphous phases. Thus, the observation of atomic structures is a key factor in this respect.

Solid-state nuclear magnetic resonance (NMR) spectroscopy is a useful characterization tool because it allows the nondestructive assessment of information about the chemical environment of chosen probe nuclei. Moreover, contrary to X-ray diffraction (XRD) and other diffraction-based techniques, solid-state NMR spectra can be successfully recorded for crystalline, nanocrystalline, or amorphous phases, allowing for the characterization of atomic environments even in structurally disordered and heterogeneous materials [24–26]. In particular, solid-state ^{27}Al NMR has been used in this way for many years in studies of SiO_2–Al_2O_3 system zeolite alumina and related materials [27–29]. In general, amorphous SiO_2–Al_2O_3 reportedly has 4-, 5-, and 6-coordinated Al [4,6], and the 4-coordinated Al is related to the acid sites of SiO_2–Al_2O_3 because it indicates Al substituted into the SiO_2 structure.

In this study, we synthesized mesoporous SiO_2–Al_2O_3 HSs using the sol–gel method under ultrasonic irradiation. Recently, various inorganic materials have been synthesized using ultrasonic irradiation [30,31]. In particular, metal oxide nanoparticles with good crystallinity have been synthesized using ultrasonic irradiation because the ultrasonic cavitation produced by ultrasonic irradiation provides a special reaction field [32–35]. In addition, we had problems with the dispersion of Al species. We tried to improve the dispersion of Al species of the SiO_2–Al_2O_3 HSs by changing the solvent and the starting material of Al_2O_3 precursors. However, there is still further improvement. Ultrasonic irradiation can improve the dispersion of the particles and its related precursors [36,37]. We can expect to increase the number of Al species into the SiO_2 structure.

Herein, we reported the effect of ultrasonic irradiation time on the morphology and physicochemical properties of mesoporous SiO_2–Al_2O_3 HSs and their activity for the hydrolysis of NH_3BH_3. Solid acids containing the mesoporous SiO_2–Al_2O_3 HSs are inexpensive compared to metal catalysts. However, the amount and rate of hydrogen generation from hydrolysis of NH_3BH_3 in the presence of solid acids exhibited low activity [38]. The mesoporous SiO_2–Al_2O_3 HSs with ultrasonic irradiation can be exhibited the high activity for hydrolysis of NH_3BH_3 because of the improved dispersion of Al leading to increase the number of acid sites. These studies may be expected to be used as a portable hydrogen source for fuel cells in the future.

2. Experiment

2.1. Synthesis of mesoporous SiO_2–Al_2O_3 HSs

Monodisperse polystyrene (PS) template particles were prepared via emulsifier-free emulsion polymerization. Specifically, styrene (27 mL, Kanto Chem. Co., >99.0 %), poly(vinyl pyrrolidone) K30 (4.50 g, Fluka, MW ≈ 40,000), cationic initiator 2,2′-azodiisobutyramidine dihydrochloride (0.78 g, Wako Pure Chemical, >97.0 %), and ion-exchanged water (300 mL) were charged into a 500-mL three-necked flask equipped with a mechanical stirrer, a nitrogen (N_2) inlet, and a Graham condenser. The reaction solution was deoxygenated by bubbling N_2 gas through the solution at room temperature for 1 h. The solution in the three-necked flask was stirred at 343 K for 24 h at 200 rpm in an oil bath with a temperature controller. The obtained white suspension was added to ion-exchanged water (180 mL) and ethanol (120 mL). This mixture suspension (40 mL) was added in centrifuge tubes and centrifuged at 3800 rpm for 10 min. Then, the centrifuged suspension was discarded and added ethanol (10 mL, Kanto Chem. Co., >99.5 %). The centrifuge tubes were shaken to disperse collected PS contents in ethanol. In addition, the centrifuge tubes were centrifuged same condition. Finally, the centrifuged suspension was discarded and the collected white content were shaken the addition of ethanol (15 mL) to obtain PS suspension. Meanwhile, cetyltrimethylammonium bromide (2.56 g, CTAB, Sigma-Aldrich, >98 %) was added to ion-exchanged water (100 mL). The solution was stirred at room temperature for 10 min to obtain a 2.5mass% aqueous CTAB solution. The obtained PS suspension (20 g), ethanol (40 mL), ion-exchanged water (100 mL), 2.5 wt% aqueous CTAB solution (5 mL), and aqueous NH_3 solution (1 mL, Kanto Chem. Co., >28.0 %–30.0 %) were stirred at room temperature for 30 min. Aluminum tri-*sec*-butoxide (11.0 μL, Kanto Chem. Co., >95.0 %) and tetraethoxysilane (389.7 μL, TEOS, Kanto Chem. Co., >99.9 %) were added to the mixed solution. The mixed suspension was stirred at 298–303 K for 3 or 6 h under ultrasonic irradiation (50 W, 40 μm) using water bath. After the suspension was dried in a desiccator overnight, mesoporous SiO_2–Al_2O_3 HSs were obtained through calcination in air at 873 K at a heating rate of 1 K min^{-1}, and these samples were cooled immediately after the designated temperature was reached (holding time for 0 h). Mesoporous SiO_2–Al_2O_3 HSs without ultrasonic irradiation were also used for comparison.

2.2. Characterization

The morphology of the samples was observed using a JEOL JEM2010F transmission electron microscope (TEM) operating at an accelerating voltage of 200 kV. The crystalline phases of the samples were determined through powder XRD using a Rigaku MultiFlex X-ray diffractometer equipped with a Ni filter and a CuKα radiation source (36 kV and 16 mA). Solid-state ^{27}Al magic angle spinning (MAS) NMR spectra were recorded on a JEOL 800-MHz wide-bore solid-state NMR system JNM-ECZ800R spectrometer (18.79 T). The relaxation delay time was 2 s, and the composites were spun at 20 kHz using a 3.2-mm ZrO_2 rotor. The chemical shift was referenced to a 1.0-M aqueous Al chloride (Wako Pure Chemical, >98.0 %) solution. The number of acid sites was measured through neutralization titration using *n*-butylamine (Kanto Chem. Co., >98.0 %).

The mesoporous SiO_2–Al_2O_3 HSs (50 mg) were dispersed in ethanol (20 mL) under sonication. The suspension was titrated with 0.1 M *n*-butylamine using methyl red (Kanto Chem. Co.) as an indicator. The number of acid sites in the samples was calculated from moles of *n*-butylamine per used sample. The N_2 adsorption isotherms of the samples were measured at 77 K using a Belsorp-18 automatic physical adsorption apparatus. Before the measurements, the samples were degassed in a vacuum at 433 K for at least 10 h. The specific surface areas of the samples were calculated using the Brunauer–Emmett–Teller (BET) method using the adsorption data. Additionally, the pore size distributions of the samples were calculated using the Barrett–Joyner–Halenda method.

2.3. Hydrolysis of NH_3BH_3

The mesoporous SiO_2–Al_2O_3 HSs (0.3 g) were placed in a two-necked round-bottom flask in air at room temperature; one neck was connected to a gas burette, and the other was connected to an addition funnel. NH_3BH_3 powder (0.0546 g, Sigma-Aldrich, 95 %) was dissolved in ion-exchanged water (40 mL) to obtain an aqueous NH_3BH_3 solution (0.044 M). The reaction was started by stirring a mixture of the sample and an aqueous NH_3BH_3 solution (5 mL). The gas evolution was monitored using the gas burette. This reaction was carried out three times in each sample.

3. Results and discussion

First, we investigated the morphology of mesoporous SiO_2–Al_2O_3 HSs using TEM measurements. Herein, mesoporous SiO_2–Al_2O_3 HSs without ultrasonic irradiation were noted under ultrasonic irradiation for 0 h. Fig. 1 shows TEM images of mesoporous SiO_2–Al_2O_3 HSs with

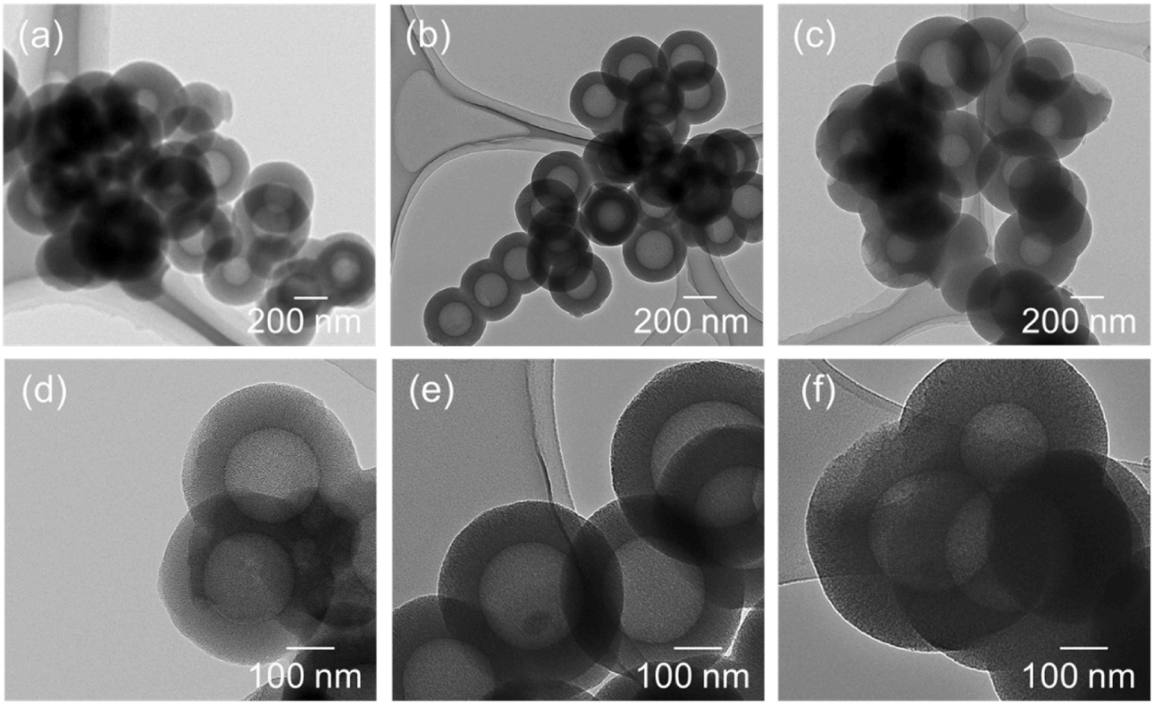

Fig. 1. TEM images of mesoporous SiO_2–Al_2O_3 hollow spheres with ultrasonic irradiation for (a) 0, (b) 3, and (c) 6 h.

various ultrasonic irradiation times. Fig. 1(a)–(c) shows that uniform HSs were observed in all samples with ultrasonic irradiation for 0, 3, and 6 h, respectively. Additionally, Fig. 1(d)–(f) demonstrates that the thicknesses of the samples with ultrasonic irradiation for 0, 3, and 6 h were approximately 100, 100, and 150 nm, respectively. According to these results, the shell thickness of the samples increased with increasing ultrasonic irradiation times. This might have been due to the presence of unreacted precursors under ultrasonic irradiation for 0 and 3 h. In the sample with ultrasonic irradiation for 6 h, the sol-gel reaction proceeds to increase shell thickness. Meanwhile, the shell thickness of the samples with ultrasonic irradiation for 0 h (stirring for 16 h at room temperature) was 100 nm, which is almost the same values as the samples with ultrasonic irradiation for 3 h. We speculated that the ultrasonic irradiation can promote the sol-gel reaction rate.

The crystalline phases of the mesoporous SiO_2–Al_2O_3 HSs were confirmed by XRD, as shown in Fig. 2. All samples showed only a broad hump at $2\theta = 15°$–$30°$, attributed to amorphous phases [39]. This suggests that the crystalline nature was not influenced by ultrasonic irradiation. Furthermore, we found that the crystalline nature did not change with increasing ultrasonic irradiation time.

We investigated the influence of ultrasonic irradiation on the crystalline natures of the mesoporous SiO_2–Al_2O_3 HSs using solid-state ^{27}Al MAS NMR with various ultrasonic irradiation times, as shown in Fig. 3. Accordingly, three peaks were observed at around 62, 35, and 5 ppm in the spectra of all the HSs, corresponding to 4-, 5-, and 6-coordinated Al species, respectively [40,41]. The 4-coordinated Al species were assigned to Al species in the silica matrix, whereas the 6-coordinated Al species were assigned to Al species outside the silica matrix [42,43]. As shown in Table 1, the ratios of the peak area of the 4-coordinated Al species in the spectra of the mesoporous SiO_2–Al_2O_3 HSs gradually increased with increasing ultrasonic irradiation time. The 4-coordinated Al species denotes Al species in the SiO_2 structure, indicating that the dispersion of Al species improved. In other words, the dispersion of Al

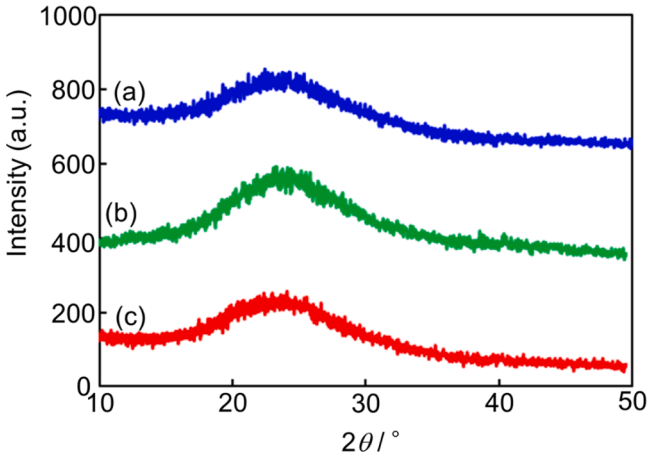

Fig. 2. XRD patterns of mesoporous SiO_2–Al_2O_3 hollow spheres with ultrasonic irradiation for (a) 0, (b) 3, and (c) 6 h.

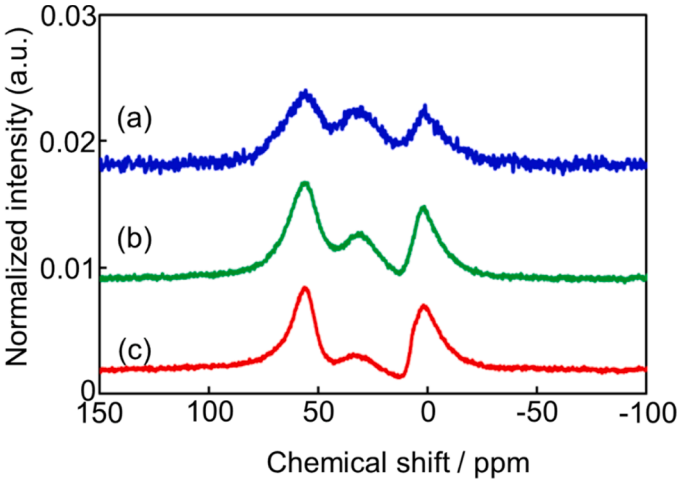

Fig. 3. ^{27}Al solid-state NMR spectra of mesoporous SiO_2–Al_2O_3 hollow spheres with ultrasonic irradiation for (a) 0, (b) 3, and (c) 6 h.

Table 1
Proportion of the peak area of mesoporous SiO_2–Al_2O_3 hollow spheres with various ultrasonic irradiation times.

Ultrasonic irradiation time	Proportion of peak area	
	4- / total	5- / total
0 h	0.38	0.35
3 h	0.43	0.33
6 h	0.51	0.12

Table 2
Number of acid sites of mesoporous SiO_2–Al_2O_3 hollow spheres with various ultrasonic irradiation times.

Ultrasonic irradiation time	Acid sites / mmol g^{-1}			
	1st	2nd	3rd	Ave
0 h	0.46	0.42	0.45	0.44
3 h	0.66	0.63	0.63	0.64
6 h	0.78	0.79	0.77	0.78

precursor can be improved by ultrasonic irradiation. Meanwhile, the ratios of the peak area of the 5-coordinated Al species in the spectra of the mesoporous SiO_2–Al_2O_3 HSs interestingly decreased with increasing ultrasonic irradiation time. Previous studies noted that 5-coordinated Al species could be attributed to amorphous phases [44,45]. This suggests that amorphous Al species can be crystallized by ultrasonic irradiation.

Finally, hydrogen generation from the hydrolysis of NH_3BH_3 was evaluated in the presence of the mesoporous SiO_2–Al_2O_3 HSs using a gas burette. Fig. 4 shows the activity for hydrolysis of NH_3BH_3 in the presence of the mesoporous SiO_2–Al_2O_3 HSs with various ultrasonic irradiation times. Herein, 7.7-, 10.6-, and 12.3-mL hydrogen were finally generated in the presence of the samples with ultrasonic irradiation for 0, 3, and 6 h, respectively. The H_2/NH_3BH_3 molar ratios of the samples with ultrasonic irradiation for 0, 3, and 6 h were calculated from the hydrogen generation as 1.4, 2.0, and 2.3, respectively. According to these results, the hydrogen evolution from the hydrolysis of NH_3BH_3 increased with increasing ultrasonic irradiation time. We speculated the reason that the H_2/NH_3BH_3 molar ratio did not achieve 3.0. This result display that the fact was not sufficient amount of acid sites to completely allow the hydrolysis of NH_3BH_3. In fact, we found that the amount of hydrogen generation increases with increase the amount of solid acids used in the hydrolysis of NH_3BH_3[22,23]. We found that the amount of hydrogen generation was dependent on the number of acid sites. The acid sites, which promotes hydrolysis of NH_3BH_3, forms when Si species in the SiO_2 structure is replaced by Al species. 4-coordinated Al species is

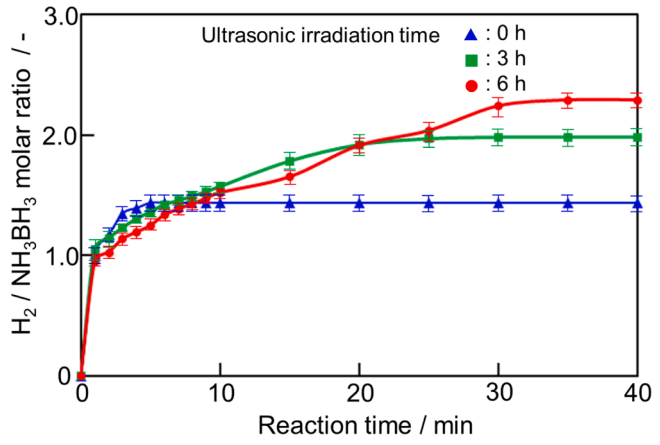

Fig. 4. Activity for hydrolysis of NH_3BH_3 in the presence of mesoporous SiO_2–Al_2O_3 hollow spheres with various ultrasonic irradiation times at room temperature.

significantly related to the acid sites because 4-coordinated Al species denote the Al species in the SiO_2 structure. Therefore, the higher proportion of 4-coordinated Al species can be considered as higher number of acid sites, thereby increasing the amount of hydrogen generation from hydrolysis of NH_3BH_3. The number of acid sites was determined in the presence of the samples using the neutralization titration method. From these results, the samples with ultrasonic irradiation for 6 h showed a high number of acid sites, and the activity for the hydrolysis of NH_3BH_3 depended on the number of acid sites. We evaluated the reusability for hydrolysis of NH_3BH_3 in the presence of mesoporous SiO_2–Al_2O_3 HSs synthesized with ultrasonic irradiation for 6 h. Fig. 5(a) shows the activity for hydrolysis of NH_3BH_3 in the presence of the reused samples with ultrasonic irradiation for 6 h. From this result, 0.1-mL hydrogen were finally generated in the presence of the reused samples with ultrasonic irradiation for 6 h (The H_2/NH_3BH_3 molar ratios was 0.01). This result indicates that the activity for hydrolysis of NH_3BH_3 were not almost promoted in the presence of the reused samples with ultrasonic irradiation for 6 h. We reveal that the number of acid sites and the proportion of 4-coordinated Al play important role in the activity for hydrolysis of NH_3BH_3. Therefore, the number of the acid sites of the reused samples with ultrasonic irradiation for 6 h was measured by the neutralization titration method. From this result, the acid sites were not existed the reused samples with ultrasonic irradiation for 6 h. Furthermore, the coordination structure of the reused samples with ultrasonic irradiation for 6 h was measured using ^{27}Al solid-state NMR. Fig. 5(b) shows ^{27}Al solid-state NMR spectra of the reused samples with ultrasonic irradiation for 6 h. The proportion of 4-coordinated Al to total coordinated Al for these samples was calculated to be 0.62. There is no significant change in the coordination structure before and after the activity for hydrolysis of NH_3BH_3. On the basis of these results, it is possible that the protons (H^+) present on the surface was consumed. The hydrolysis reaction proceeds to form ammonium ion (NH_4^+) and these NH_4^+ might be replaced by H^+, it is inferred that the acid sites were not function.

Meanwhile, the reaction times to complete the hydrogen generation were within 5, 30, and 35 min, indicating that the reaction time to final hydrogen evolution increased with increasing ultrasonic irradiation time. To investigate this difference, we measured the pore size distribution of the samples using N_2 adsorption–desorption measurement. Fig. 6 shows the pore size distribution of the samples. The samples with ultrasonic irradiation for 0 and 3 h had peaks at 2.4 and 2.1 nm, suggesting that these samples had many mesopores. Meanwhile, the sample with ultrasonic irradiation for 6 h had a peak at a value smaller than approximately 1.4 nm. According to these results, the mesopore size of the samples decreased with increasing ultrasonic irradiation time. This result may be because mesopores were not formed by ultrasonic irradiation.

Furthermore, Table 3 shows the BET specific surface area of the samples. The values for the samples with ultrasonic irradiation for 0 and 3 h were 961 and 938 $m^2\ g^{-1}$, indicating almost the same BET specific surface areas, whereas the sample with ultrasonic irradiation for 6 h showed a decrease to 688 $m^2\ g^{-1}$. These results may also be attributed to a decrease in the number of mesopores formed in the shells of the HSs. For the mesoporous SiO_2-Al_2O_3 HSs, rod-shaped micelles were first formed on the surface of PS particles, and then the mesoporous SiO_2-Al_2O_3 shells were formed by sol-gel method with ultrasound irradiation. Previous studies reported that the micelles were decomposed by cavitation formed by ultrasound irradiation [46,47]. We considered that the formation of uniform mesopores for the samples with ultrasonic irradiation was not possible due to the collapse of the micelles on the surface of PS particles. In fact, the reaction time to complete hydrogen generation of the samples with ultrasonic irradiation for 0 h were faster than ultrasonic irradiation for 3 and 6 h, probably because have the uniform pores from the results of pore size distribution. Meanwhile the samples with ultrasonic irradiation for 3 and 6 h may be formed the disordered and/or collapsed pores based on the result of pore size distribution.

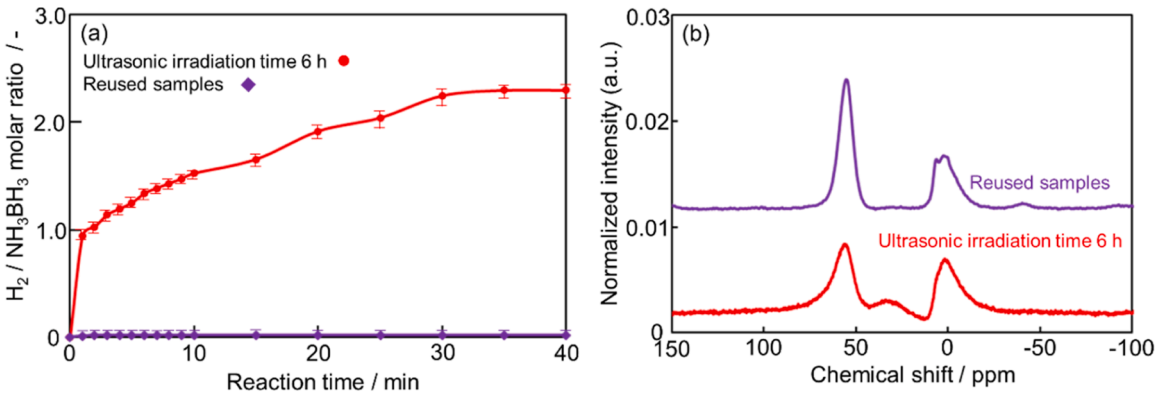

Fig. 5. (a) Activity for hydrolysis of NH_3BH_3 and (b) ^{27}Al solid-state NMR spectra of the reused mesoporous SiO_2–Al_2O_3 hollow spheres with ultrasonic irradiation for 6 h.

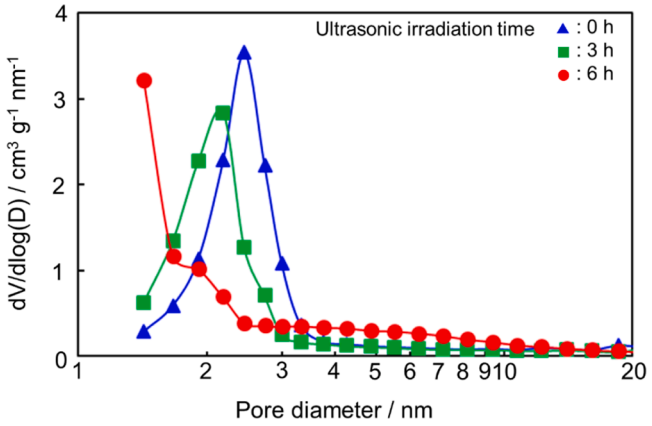

Fig. 6. Pore size distributions of mesoporous SiO_2–Al_2O_3 hollow spheres with various ultrasonic irradiation times.

Table 3
BET specific surface area of mesoporous SiO_2–Al_2O_3 hollow spheres with various ultrasonic irradiation times.

Ultrasonic irradiation time	BET specific surface area / $m^2\ g^{-1}$
0 h	961
3 h	931
6 h	688

Additionally, the shell thickness of the samples with ultrasonic irradiation for 6 h was approximately 150 nm from the result of TEM images, and the mesoporous SiO_2-Al_2O_3 shells may be also formed on micelles. We considered that combination of these factors effect on the diffusion of NH_3BH_3 to the acid sites.

4. Conclusion

In this study, mesoporous SiO_2–Al_2O_3 HSs were synthesized using ultrasonic irradiation, and their samples were evaluated using the hydrolysis of NH_3BH_3. Uniform HSs were observed in the TEM images of samples with ultrasonic irradiation for 0, 3, and 6 h. The shell thickness of the samples increased with increasing ultrasonic irradiation time. ^{27}Al solid-state NMR spectra showed that the proportion of 5-coordinated Al species attributed to amorphous Al species decreased and the proportion of 4-coordinated Al species attributed to Al species in the SiO_2 structure increased as the ultrasonic irradiation time increased. These samples were evaluated in terms of their activity for the hydrolysis of NH_3BH_3. This result revealed that increasing the ultrasonic irradiation time increases the amount of hydrogen evolution from the hydrolysis of NH_3BH_3 due to the improved dispersion of Al species leading to increase the number of acid sites. On the other hand, the reaction time to complete hydrogen generation increased with increasing ultrasonic irradiation time due to the decrease the number of mesopores and thicker shell thickness. To improve this problem, the samples with thinner shell thickness may lead to faster hydrogen generation rate and development of practical applications.

Declaration of Competing Interest

The authors declare that they have no known competing financial interests or personal relationships that could have appeared to influence the work reported in this paper.

Acknowledgements

This work was supported by NIMS Joint Research Hub Program (Grant number 2024–024) and "Advanced Research Infrastructure for Materials and Nanotechnology in Japan (ARIM)" of the Ministry of Education, Culture, Sports, Science and Technology (MEXT) (Grant Number JPMXP1224NM0107 and JPMXP1224UT0184). We are grateful to Mr. Oshikawa (Univ. of Tokyo) for using the TEM measurement.

References

[1] A. Corma, Inorganic solid acids and their use in acid-catalyzed hydrocarbon reactions, Chem. Rev. 95 (1995) 559–614, https://doi.org/10.1021/cr00035a006.
[2] G. Busca, Acid catalysts in industrial hydrocarbon chemistry, Chem. Rev. 107 (2007) 5366–5410, https://doi.org/10.1021/cr068042e.
[3] A.J.G.Julius Scherzer, Hydrocracking Science and Technology, Marcel Dekker, New York, 1996.
[4] E.J.M. Hensen, D.G. Poduval, P.C.M.M. Magusin, A.E. Coumans, J.A.Rv Veen, Formation of acid sites in amorphous silica-alumina, J. Catal. 269 (2010) 201–218, https://doi.org/10.1016/j.jcat.2009.11.008.
[5] M. Trombetta, G. Busca, S. Rossini, V. Piccoli, U. Cornaro, A. Guercio, R. Catani, R. J. Willey, FT-IR studies on light olefin skeletal isomerization catalysis: III. surface acidity and activity of amorphous and crystalline catalysts belonging to the SiO2-Al2O3 system, J. Catal. 179 (1998) 581–596, https://doi.org/10.1006/jcat.1998.2251.
[6] E.J.M. Hensen, D.G. Poduval, V. Degirmenci, D.A.J.M. Ligthart, W. Chen, F. Maugé, M.S. Rigutto, J.A.Rv Veen, Acidity characterization of amorphous silica-alumina, J. Phys. Chem. C. 116 (2012) 21416–21429, https://doi.org/10.1021/jp309182f.
[7] N. Toyama, T. Umegaki, Y. Kojima, Fabrication of hollow silica-alumina composite spheres and their activity for hydrolytic dehydrogenation of ammonia borane, Int. J. Hydrog. Energy 39 (2014) 17136–17143, https://doi.org/10.1016/j.ijhydene.2014.08.057.
[8] N. Toyama, T. Umegaki, Y. Kojima, Influence of Si/Al molar ratio of hollow silica-alumina composite spheres on their activity for hydrolytic dehydrogenation of ammonia borane, Int. J. Hydrog. Energy 40 (2015) 6151–6157, https://doi.org/10.1016/j.ijhydene.2015.03.021.
[9] C.W. Hamilton, R.T. Baker, A. Staubitz, I. Manners, B–N compounds for chemical hydrogen storage, Chem. Soc. Rev. 38 (2009) 279–293, https://doi.org/10.1039/b800312m.

[10] U.B. Demirci, Ammonia borane, a material with exceptional properties for chemical hydrogen storage, Int. J. Hydrog. Energy 42 (2017) 9978–10013, https://doi.org/10.1016/j.ijhydene.2017.01.154.
[11] S. Akbayrak, S. Özkar, Ammonia borane as hydrogen storage materials, Int. J. Hydrog. Energy 43 (2018) 18592–18606, https://doi.org/10.1016/j.ijhydene.2018.02.190.
[12] X. Feng, Y. Zhao, D. Liu, Y. Mo, Y. Liu, X. Chen, W. Yan, X. Jin, B. Chen, X. Duan, D. Chen, C. Yang, Towards high activity of hydrogen production from ammonia borane over efficient non-noble Ni5P4 catalyst, Int. J. Hydrog. Energy 43 (2018) 17112–17120, https://doi.org/10.1016/j.ijhydene.2018.07.055.
[13] J. Sun, W. Zhang, H. Li, J. Liu, Z. Xu, S. Zheng, Size-tunable Ni particles confined in the ordered mesoporous silica for catalytic H2 production from ammonia borane hydrolysis, Int. J. Hydrog. Energy 58 (2024) 964–973, https://doi.org/10.1016/j.ijhydene.2024.01.233.
[14] H. Wu, Y. Cheng, Y. Fan, X. Lu, L. Li, B. Liu, B. Li, S. Lu, Metal-catalyzed hydrolysis of ammonia borane: mechanism, catalysts, and challenges, Int. J. Hydrog. Energy 45 (2020) 30325–30340, https://doi.org/10.1016/j.ijhydene.2020.08.131.
[15] K. Wang, Y. Chen, S. Li, K. Feng, S. Wang, J. Zhong, Self-reconstructed Co-B active sites for high-efficiency hydrolysis of ammonia borane, ACS Mater. Lett. 5 (2023) 1188–1195, https://doi.org/10.1021/acsmaterialslett.3c00165.
[16] M. Asim, S. Zhang, Y. Wang, B. Maryam, M. Sajid, C. Shi, L. Pan, X. Zhang, J. Zou, Self-supporting NiCoP for hydrogen generation via hydrolysis of ammonia borane, Fuel 318 (2022) 123544, https://doi.org/10.1016/j.fuel.2022.123544.
[17] J. Liao, Y. Wu, Y. Shao, Y. Feng, X. Zhang, W. Zhang, J. Li, M. Wu, H. Dong, Q. Liu, H. Li, Ammonia borane methanolysis for hydrogen evolution on $Cu_3Mo_2O_9$/$NiMoO_4$ hollow microspheres, Chem. Eng. J. 449 (2022) 137755, https://doi.org/10.1016/j.cej.2022.137755.
[18] Y. Feng, Y. Li, Q. Liao, W. Zhang, Z. Huang, X. Chen, Y. Shao, H. Dong, Q. Liu, H. Li, Modulation the electronic structure of hollow structured CuO-$NiCo_2O_4$ nanosphere for enhanced catalytic activity towards methanolysis of ammonia borane, Fuel 332 (2023) 126045, https://doi.org/10.1016/j.fuel.2022.126045.
[19] Y. Li, J. Liao, Y. Feng, J. Li, Q. Liu, W. Zhou, M. He, H. Li, Built-in Electric Field in Yolk Shell CuO-Co3O4@Co3O4 with modulated interfacial charge to facilitate hydrogen production from ammonia borane methanolysis under visible light, Adv. Funct. Mater. 34 (2024) 2405361, https://doi.org/10.1002/adfm.202405361.
[20] J. Liao, Y. Li, J. Tian, Y. Feng, Q. Liu, H. Li, Morphology engineering of hollow core@shell structured Co_3O_4@CuO-NiO for fast hydrogen release from ammonia borane methanolysis, J. Colloid Inter. Sci. 680 (2025) 78–87, https://doi.org/10.1016/j.jcis.2024.10.177.
[21] N. Toyama, S. Ohki, M. Tansho, T. Shimizu, T. Umegaki, Y. Kojima, Influence of morphology of Silica-Alumina composites on their activity for hydrolytic dehydrogenation of ammonia borane, J. Jpn. Inst. Energy 95 (2016) 480–486, https://doi.org/10.3775/jie.95.480.
[22] N. Toyama, N. Nikura, I. Ito, T. Umegaki, Y. Kojima, Synthesis of mesoporous silica-zirconia composite hollow spheres with enhanced activity toward hydrolysis of ammonia borane, Microporous Mesoporous Mater. 294 (2020) 109839, https://doi.org/10.1016/j.micromeso.2019.109839.
[23] N. Toyama, S. Ohki, M. Tansho, T. Shimizu, T. Umegaki, Y. Kojima, Influence of aluminum precursors on structure and acidic properties of hollow silica-alumina composite spheres, and their activity for hydrolytic dehydrogenation of ammonia borane, Int. J. Hydrog. Energy 42 (2017) 22318–22324, https://doi.org/10.1016/j.ijhydene.2017.05.128.
[24] J.C.C. Freitas, A.Gd Cunha, F.G. Emmerich, Solid-State nuclear magnetic resonance (NMR) methods applied to the study of carbon materials, Comb. Probab. Comput. (2012) 85–170, https://doi.org/10.1201/b12960-3.
[25] M.E.S. Kenneth, J.D. MacKenzie, Multinuclear Solid-State Nuclear Magnetic Resonance of Inorganic Materials, Pergamon, Oxford, 2002.
[26] T.R. Lopes, G.R. Gonçalves, E. de Barcellos, M.A. Schettino, A.G. Cunha, F. G. Emmerich, J.C.C. Freitas, Solid state ^{27}Al NMR and X-ray diffraction study of alumina-carbon composites, Carbon 93 (2015) 751–761, https://doi.org/10.1016/j.carbon.2015.06.001.
[27] R. Hajjar, Y. Millot, P.P. Man, M. Che, S. Dzwigaj, Two kinds of framework Al sites studied in BEA zeolite by X-ray diffraction, fourier transform infrared spectroscopy, NMR techniques, and V probe, J. Phys. Chem. C. 112 (2008) 20167–20175, https://doi.org/10.1021/jp808356q.
[28] S.M. Maier, A. Jentys, J.A. Lercher, Steaming of zeolite BEA and its effect on acidity: a comparative NMR and IR spectroscopic study, J. Phys. Chem. C. 115 (2011) 8005–8013, https://doi.org/10.1021/jp108338g.
[29] N. Kondo, T. Tatsumi, Control of the Al distribution in the framework of ZSM-5 zeolite and its evaluation by solid-state NMR technique and catalytic properties, J. Phys. Chem. C. 119 (2015) 15303–15315, https://doi.org/10.1021/acs.jpcc.5b03289.
[30] M. Ismael, One-step ultrasonic-assisted synthesis of Ni-doped g-C_3N_4 photocatalyst for enhanced photocatalytic hydrogen evolution, Inorg. Chem. Commun. 151 (2023) 110607, https://doi.org/10.1016/j.inoche.2023.110607.
[31] W.A. Freitas, B.E.C.F. Soares, M.S. Rodrigues, P. Trigueiro, L.M.C. Honorio, R. Peña-Garcia, A.C.S. Alcântara, E.C. Silva-Filho, M.G. Fonseca, M.B. Furtini, J. A. Osajima, Facile synthesis of ZnO-clay minerals composites using an ultrasonic approach for photocatalytic performance, J. Photochem. Photobiol., A 429 (2022) 113934, https://doi.org/10.1016/j.jphotochem.2022.113934.
[32] R.V. Kumar, Y. Diamant, A. Gedanken, Sonochemical synthesis and characterization of nanometer-size transition metal oxides from metal acetates, Chem. Mater. 12 (2000) 2301–2305, https://doi.org/10.1021/cm000166z.
[33] K.V.P.M. Shafi, A. Ulman, X. Yan, N.-L. Yang, C. Estournès, H. White, M. Rafailovich, Sonochemical synthesis of functionalized amorphous iron oxide nanoparticles, Langmuir 17 (2001) 5093–5097, https://doi.org/10.1021/la010421.
[34] S. Askari, S. Miar Alipour, R. Halladj, M.H. Davood Abadi Farahani, Effects of ultrasound on the synthesis of zeolites: a review, J. Porous Mater. 20 (2013) 285–302, https://doi.org/10.1007/s10934-012-9598-6.
[35] D. Vaičiukynienė, A. Kantautas, V. Vaitkevičius, L. Jakevičius, Ž. Rudžionis, M. Paškevičius, Effects of ultrasonic treatment on zeolite NaA synthesized from by-product silica, Ultrason. Sonochem. 27 (2015) 515–521, https://doi.org/10.1016/j.ultsonch.2015.06.001.
[36] C.W. Wong, Y.S. Chan, J. Jeevanandam, K. Pal, M. Abd Elkodous, G.S. El-Sayyad, Response surface methodology optimization of mono-dispersed MgO nanoparticles fabricated by ultrasonic-assisted sol–gel method for outstanding antimicrobial and antibiofilm activities, J. Clust. Sci. 31 (2020) 367–389, https://doi.org/10.1007/s10876-019-01651-3.
[37] M.L. Tsai, S.W. Bai, R.H. Chen, Cavitation effects versus stretch effects resulted in different size and polydispersity of ionotropic gelation chitosan–sodium tripolyphosphate nanoparticle, Carbohyd. Polym. 71 (2008) 448–457, https://doi.org/10.1016/j.carbpol.2007.06.015.
[38] M. Chandra, Q. Xu, Dissociation and hydrolysis of ammonia-borane with solid acids and carbon dioxide: an efficient hydrogen generation system, J. Power Sources 159 (2006) 855–860, https://doi.org/10.1016/j.jpowsour.2005.12.033.
[39] F. Hao, J. Zhong, P.-L. Liu, K.-Y. You, H.-A. Luo, Amorphous SiO_2-Al_2O_3 supported Co_3O_4 and its catalytic properties in cyclohexane nitrosation to ε-caprolactam: influences of preparation conditions, J. Mol. Catal. A 363 (2012) 41–48, https://doi.org/10.1016/j.molcata.2012.05.014.
[40] X. Fang, Z. Liu, M.-F. Hsieh, M. Chen, P. Liu, C. Chen, N. Zheng, Hollow mesoporous aluminosilica spheres with perpendicular pore channels as catalytic nanoreactors, ACS Nano 6 (2012) 4434–4444, https://doi.org/10.1021/nn3011703.
[41] A.J.J. Koekkoek, J.A.R. van Veen, P.B. Gerrtisen, P. Giltay, P.C.M.M. Magusin, E.J. M. Hensen, Brønsted acidity of Al/SBA-15, Microporous Mesoporous Mater. 151 (2012) 34–43, https://doi.org/10.1016/j.micromeso.2011.11.019.
[42] J. Zhuang, D. Ma, G. Yang, Z. Yan, X. Liu, X. Liu, X. Han, X. Bao, P. Xie, Z. Liu, Solid-state MAS NMR studies on the hydrothermal stability of the zeolite catalysts for residual oil selective catalytic cracking, J. Catal. 228 (2004) 234–242, https://doi.org/10.1016/j.jcat.2004.08.034.
[43] A. Sakthivel, S.E. Dapurkar, N.M. Gupta, S.K. Kulshreshtha, P. Selvam, The influence of aluminium sources on the acidic behaviour as well as on the catalytic activity of mesoporous H-AlMCM-41 molecular sieves, Microporous Mesoporous Mater. 65 (2003) 177–187, https://doi.org/10.1016/j.micromeso.2003.08.004.
[44] H. Hashimoto, K. Yazawa, H. Asoh, S. Ono, NMR spectroscopic analysis of the local structure of porous-type amorphous alumina prepared by anodization, J. Phys. Chem. C. 121 (2017) 12300–12307, https://doi.org/10.1021/acs.jpcc.7b03629.
[45] V. Sarou-Kanian, A.N. Gleizes, P. Florian, D. Samélor, D. Massiot, C. Vahlas, Temperature-Dependent 4-, 5- and 6-Fold coordination of aluminum in MOCVD-grown amorphous alumina films: a very high field 27Al-NMR study, J. Phys. Chem. C. 117 (2013) 21965–21971, https://doi.org/10.1021/jp4077504.
[46] B. Cai, J. Mazahreh, Q. Ma, F. Wang, X. Hu, Ultrasound-assisted fabrication of biopolymer materials: a review, Int. J. Biol. Macromol. 209 (2022) 1613–1628, https://doi.org/10.1016/j.ijbiomac.2022.04.055.
[47] X. Liu, K. Zhao, J. Cao, X. Qi, L. Wu, S. Shen, Ultrasound responsive self-assembled micelles loaded with hypocrellin for cancer sonodynamic therapy, Int. J. Pharm. 608 (2021) 121052, https://doi.org/10.1016/j.ijpharm.2021.121052.